Proinflammatory cytokine-induced tight junction remodeling through dynamic self-assembly of claudins

Christopher T. Capaldo[a], Attila E. Farkas[a], Roland S. Hilgarth[a], Susanne M. Krug[b], Mattie F. Wolf[a], Jeremy K. Benedik[a], Michael Fromm[b], Michael Koval[c], Charles Parkos[a], and Asma Nusrat[a]

[a]Epithelial Pathobiology and Mucosal Inflammation Research Unit, Department of Pathology and Laboratory Medicine, and [c]Division of Pulmonary, Allergy and Critical Care Medicine, Department of Cell Biology, Emory University, Atlanta, GA 30322; [b]Institute of Clinical Physiology Charité, Campus Benjamin Franklin, Freie Universität and Humboldt-Universität, 12200 Berlin, Germany

ABSTRACT **Tight junctions (TJs) are dynamic, multiprotein intercellular adhesive contacts that provide a vital barrier function in epithelial tissues. TJs are remodeled during physiological development and pathological mucosal inflammation, and differential expression of the claudin family of TJ proteins determines epithelial barrier properties. However, the molecular mechanisms involved in TJ remodeling are incompletely understood. Using acGFP-claudin 4 as a biosensor of TJ remodeling, we observed increased claudin 4 fluorescence recovery after photobleaching (FRAP) dynamics in response to inflammatory cytokines. Interferon γ and tumor necrosis factor α increased the proportion of mobile claudin 4 in the TJ. Up-regulation of claudin 4 protein rescued these mobility defects and cytokine-induced barrier compromise. Furthermore, claudins 2 and 4 have reciprocal effects on epithelial barrier function, exhibit differential FRAP dynamics, and compete for residency within the TJ. These findings establish a model of TJs as self-assembling systems that undergo remodeling in response to proinflammatory cytokines through a mechanism of heterotypic claudin-binding incompatibility.**

Monitoring Editor
David G. Drubin
University of California, Berkeley

Received: Feb 26, 2014
Revised: Jul 8, 2014
Accepted: Jul 9, 2014

INTRODUCTION

Tight junctions (TJs) are the apicalmost intercellular junction and regulate movement of fluids and molecules between cells. They are composed of anastomosing proteinaceous strands that span the extracellular space to form a regulatable seal between adjacent cells. The molecular composition of the TJ is complex, consisting of multiple integral membrane and cytosolic proteins (Tsukita and Furuse, 2002; Furuse, 2010; Anderson and Van Itallie, 2009).

The integral membrane proteins that comprise the TJ include claudins—requisite components that dictate TJ barrier properties. The variety and proportion of claudin polymers present in the TJ determine barrier tightness, strand architecture, and paracellular ion permeability (Claude and Goodenough, 1973; Rahner *et al.*, 2001; Anderson and Van Itallie, 2009; Shen *et al.*, 2011). For example, claudin 4 protein is a TJ-sealing claudin and expression correlates with tight epithelial tissues and restricted sodium flux (Van Itallie *et al.*, 2001). In contrast, claudin 2 is a pore-forming claudin that confers a leaky-strand phenotype and increased junction permeability (Furuse *et al.*, 2001). Structurally, claudin gene products generate four pass transmembrane proteins with two predicted extracellular loops. There are as many as 27 claudin genes in humans, whose primary extracellular loop structure determines the ion and charge selectivity of the resultant TJ paracellular pores (Daugherty *et al.*, 2007; Piontek *et al.*, 2008; Anderson and Van Itallie, 2009). Furthermore, primary loop structure determines claudin–claudin interactions both within and between opposing plasma membranes (Daugherty *et al.*, 2007; Piontek *et al.*, 2011).

Proinflammatory cytokine exposure during mucosal inflammation disrupts physiological epithelial TJ structure and composition,

This article was published online ahead of print in MBoC in Press (http://www.molbiolcell.org/cgi/doi/10.1091/mbc.E14-02-0773) on July 16, 2014.

The authors have no conflicts of interest.

Address correspondence to: A. Nusrat (anusrat@emory.edu).

Abbreviations used: acGFP, *Aequorea coerulescens* green fluorescent protein; CMV, cytomegalovirus; FRAP, fluorescence recovery after photobleaching; GBP-1, guanylate-binding protein 1; IEC, intestinal epithelial cell; IFN-γ, interferon γ; NFκB, nuclear factor κB; ROI, region of interest; TER, transepithelial electrical resistance; TJ, tight junction; TNF-α, tumor necrosis factor α.

resulting in increased paracellular permeability (Capaldo and Nusrat, 2009). However, the molecular mechanisms that drive TJ reorganization in such inflammatory states are not well understood. Intestinal epithelial cells differentially express claudin protein family members along crypt luminal axis. Claudin 4 is expressed in luminal epithelial cells, which have a tight barrier, whereas basal crypt epithelial cells express claudin 2 (Rahner *et al.*, 2001). Such claudin protein gradients are perturbed in compromised epithelial barriers during mucosal inflammation. For example, claudin 2 is increased during mucosal inflammation and confers a leaky junction phenotype, whereas claudin 4 has been reported to be reduced and promotes a tight barrier (Prasad *et al.*, 2005; Zeissig *et al.*, 2007; Wray *et al.*, 2009; Mitchell *et al.*, 2011). To study the mechanisms of proinflammatory cytokine-mediated compromise of TJs, we focused on a TJ claudin protein family member, claudin 4. Claudin 4 was selected because its expression correlates with mature TJs and tight tissue barriers. Furthermore, mucosal inflammation is associated with decreased claudin 4 (Prasad *et al.*, 2005; Hering *et al.*, 2012). We therefore hypothesized that cytokine-induced TJ remodeling is associated with increased claudin 4 dynamics at the TJ.

To test this hypothesis, we generated model intestinal epithelial cells (IECs) stably expressing *Aequorea coerulescens* green fluorescent protein (acGFP)–claudin 4 and assessed claudin 4 mobility by fluorescence recovery after photobleaching (FRAP) as a biosensor of TJ remodeling. Although previous studies investigated the dynamics of TJ proteins by FRAP, the relationship between epithelial TJ structure/function, TJ protein kinetics, and remodeling during mucosal inflammation is not understood (Sasaki *et al.*, 2003; Shen *et al.*, 2008, 2011; Piontek *et al.*, 2011; Yamazaki *et al.*, 2011). In this study we analyzed the influence of interferon γ (IFN-γ) and tumor necrosis factor α (TNF-α), proinflammatory cytokines that are elevated in inflamed mucosal tissues (Mankertz and Schulzke, 2007). By FRAP analysis, IFN-γ/TNF-α increased the mobile fraction of TJs localized acGFP-claudin 4, yet cytokine signaling did not alter acGFP-claudin 4 mobile pool exchange dynamics. Simultaneous up-regulation of claudin 4 protein levels during IFN-γ/TNF-α treatment stabilized the immobile claudin 4 subpool, suppressed claudin 2 levels, and rescued IEC barrier defects. In contrast to claudin 4, dynamics of the pore-forming claudin 2 were decreased after cytokine treatment, showing claudin isoform–specific sensitivity. From our data we conclude that proinflammatory cytokines remodel TJs, and contribute to epithelial barrier dysfunction, by decreasing assembly of claudin 4 into TJs.

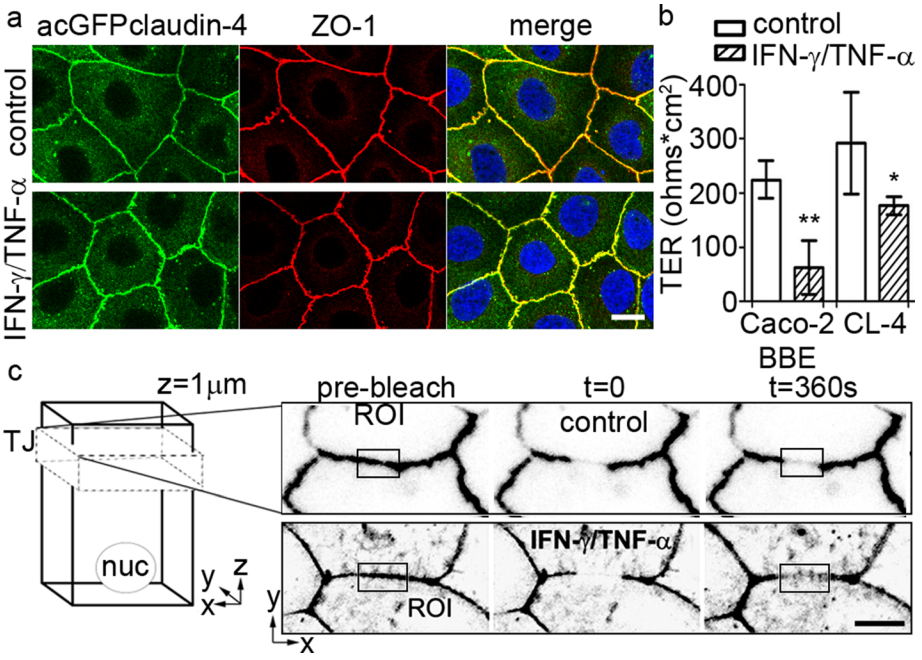

FIGURE 1: Proinflammatory cytokines IFN-γ/TNF-α increase claudin 4 mobility within the TJ. (a) Caco-2 BBEs expressing acGFP-claudin 4 under nontreated control conditions or after 48 h treatment with cytokines (bar, 10 μm). (b) TER measurements in parental Caco-2 BBE cells and Caco-2 BBE cells stably expressing acGFP claudin 4 (CL-4) under nontreated control conditions or after 48 h treatment with IFN-γ/TNF-α. SEM, $n = 3$; CL-4 + cytokine vs. all conditions, $^*p < 0.05$; Caco-2 BBE + cytokine vs. all conditions, $^{**}p < 0.01$, by ANOVA. (c) Schematic depicting columnar IECs. Tight junction structures are near the apex of the lateral surface (TJ). Live-cell confocal imaging was performed in this region with an optical *z*-slice of ~1 μm. Selected time-lapse confocal images of Caco-2 BBE IECs expressing acGFP-claudin 4 are shown, with ROIs subjected to FRAP either under control conditions or after 48 h IFN-γ/TNF-α treatment. Images were converted to grayscale and inverted to enhance contrast (bar, 5 μm).

RESULTS

Proinflammatory cytokines IFN-γ and TNF-α increase claudin 4 TJ dynamics

To investigate mechanisms by which proinflammatory cytokines IFN-γ and TNF-α compromise IEC TJs, we used the fluorescence recovery after photobleaching (FRAP) technique to analyze the dynamic behavior of claudin 4 in TJs (Sasaki *et al.*, 2003; Shen *et al.*, 2008; Yamazaki *et al.*, 2011; Yu *et al.*, 2010). We generated an N-terminal–tagged fluorescent claudin 4 fusion construct using *Aequorea coerulescens* green fluorescent protein (acGFP), due to its photostability, brightness, and monomeric properties (Shen *et al.*, 2008; Raleigh *et al.*, 2011). Custom expression vectors were also designed, as conventional vectors contain viral promoter elements that increase activity in response to cytokines (Kline *et al.*, 1998; Gilham *et al.*, 2010). Four nuclear factor κB (NFκB) *cis*-elements were mutated within a cytomegalovirus promoter sequence, thereby ablating cytokine-responsive stimulation of protein expression (pRol; Supplemental Figure S1, a and b). This construct was stably expressed in the model intestinal epithelial cell line Caco-2 BBE and used in subsequent experiments unless otherwise indicated. AcGFP-claudin 4 expression and TJ targeting were then confirmed by confocal microscopy (Figure 1a).

As shown in Figure 1a, acGFP-claudin 4 is targeted to cell contacts and colocalizes with the TJ plaque protein ZO-1. Both cell–cell contact and ZO-1/acGFP-claudin 4 colocalization were maintained after 48-h treatment with the proinflammatory cytokines IFN-γ/TNF-α, subsequently referred to as cytokine treatment (Figure 1a). Despite the maintenance of TJ integrity, Caco-2 BBE barrier function was compromised in cytokine-treated epithelial cells (Figure 1b). IEC barrier function was measured by transepithelial electrical resistance (TER), and a significant reduction in barrier function was found after cytokine exposure. Consistent with previous reports, expression of claudin 4 enhanced IEC barrier function under baseline conditions (Van Itallie *et al.*, 2001). Surprisingly, expression of exogenous

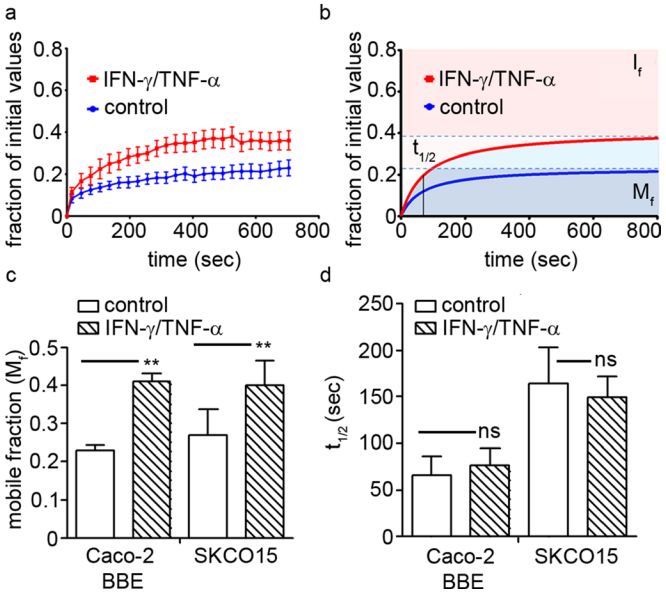

FIGURE 2: The proinflammatory cytokines IFN-γ/TNF-α alter the proportion of claudin 4 between mobile and immobile TJ subpools. (a) FRAP ROI pixel intensity over time in either nontreated control conditions or after IFN-γ/TNF-α treatment. (b) Best fit curves and nonlinear regression analysis used to determine the half-life of recovery ($t_{1/2}$) and the plateau of maximum fluorescence recovery (I_{max}, dashed line). (c) Proportions of M_f and I_f. Claudin 4 mobile fraction values increase with cytokine exposure (SEM, $^{**}p < 0.01$: Caco-2, $n = 13/10$; SKCO15, $n = 8/9$; ANOVA; all other comparisons are not significant [ns]). (d) Half-life of recovery ($t_{½}$) is not altered by cytokine treatment.

claudin 4 ameliorated cytokine-induced barrier loss (Figure 1b). The above findings show that acGFP-claudin 4 is targeted to TJ structures and acts to regulate barrier function. To assess the effects of cytokine stimulation on claudin 4 dynamics, we treated acGFP-claudin 4–expressing Caco-2 BBE cells with IFN-γ/TNF-α for 48 h, after which we assessed claudin 4 mobility by live-cell confocal microscopy and FRAP (Figure 1c). We observed increased claudin 4 fluorescence recovery in cytokine-treated cells as compared with nontreated controls, indicating cytokine-induced changes in claudin 4 protein dynamics. However, this was not due to increased diffusion of claudin 4 within the plane of the junction (planar diffusion; Supplemental Video S1). Indeed, kymograph analysis of bleached TJs did not show evidence of planar claudin 4 mobility in either condition, indicating that fluorescence recovery proceeds from a lateral plasma membrane subpool (Supplemental Figure S2a; see later discussion of Figure 8).

Cytokine exposure decreases the ratio of immobile to mobile claudin 4

To explore mechanisms of cytokine-induced increases in claudin 4 mobility, we recorded photobleached TJ regions of interest (ROIs) for pixel intensity over the extent of the experiment and plotted them as shown in Figure 2a. Mathematical modeling and nonlinear regression analysis were then performed. Half-time of recovery ($t_{1/2}$) and maximum recovery plateau (I_{max}, dashed line) of the resulting pixel intensity profiles are illustrated in Figure 2b. Pixel intensity maximum recovery values were then used to calculate the proportion of mobile (recovered subpool, M_f) and immobile (nonrecovered subpool, I_f) acGFP-claudin 4 within the TJ in both the baseline state and after cytokine exposure (Figure 2c). Similar to previous studies of claudin mobility (Raleigh *et al.*, 2011), claudin 4 shows limited mobility within the junction under control conditions, with a low proportion of mobile claudin 4 (M_f, Figure 2c, Supplemental Table S1). However, cytokine treatment induced a significant increase in the proportion of mobile claudin 4. Of interest, no significant difference in $t_{1/2}$ could be determined between nontreated control and cytokine-exposed IECs (Figure 2d). Complementary results were obtained using an additional model IEC cell line, SKCO15, which exhibited a higher $t_{1/2}$ than Caco-2 BBEs, indicating slower recovery rates. However, we determined dramatic alterations in SKCO15 claudin 4 mobile/immobile pool proportions and no determinable change in mobile pool $t_{1/2}$ values between control and cytokine-treated cultures. Unlike Caco-2 cells, SKCO15 cells respond to IFN-γ in the baseline state (Chavez *et al.*, 1999; Wang *et al.*, 2005). Indeed, in SKCO15 cells, treatment with either cytokine alone was sufficient to increase the mobile pool of claudin 4 within the TJ (Supplemental Figure S2b). Whereas we observed cell type variability in $t_{1/2}$ between Caco-2 and SKCO15 cells, the $t_{1/2}$ of mobile pool exchange in response to cytokine treatment was similar to controls in both model intestinal epithelial cell lines (Supplemental Figure S2, c and d). In agreement with our Caco-2 BBE data, planar diffusion was not observed under these experimental conditions (Supplemental Figure S2a). The foregoing data indicate that cytokine exposure alters the proportion of immobile/mobile claudin 4 within the TJ but does not alter the rate of mobile pool exchange. On the basis of these findings we focused on understanding the nature of cytokine-induced changes to the claudin 4 immobile/mobile fraction, which could be due to 1) an increase in mobile claudin 4, 2) a decrease in immobile claudin 4, or 3) a combination of these two events.

Cytokines act to decrease TJ-integrated immobile claudin 4

To investigate mechanisms that regulate the partitioning of claudin 4 into mobile/immobile FRAP subpools, we explored the nature of these subpools in greater detail. We speculated that an increase in mobile claudin 4, without a change in immobile claudin 4, would be reflected in an increase in total protein levels. However, an assessment of claudin 4 protein levels by Western blot revealed a decrease in total endogenous claudin 4 after cytokine treatment (Figure 3a and Supplemental Figure S4). This finding would suggest that cytokine-induced mobility changes are due in part to decreased immobile claudin 4. Recent reports on TJ protein dynamics proposed that the immobile fraction (I_f) represents claudin protein that is stably integrated into the TJ; conversely, mobile fraction (M_f) subpools are peripheral to the junction (Shen *et al.*, 2008). To test this possibility directly, we analyzed claudin 4 mobility after inhibition of protein synthesis, which we hypothesized would result in reduced mobile claudin 4. Endogenous claudin 4 protein degradation kinetics was evaluated after protein synthesis inhibition with cycloheximide. As shown in Figure 3b, endogenous claudin 4 protein is rapidly degraded to ~50% of initial levels, (2–4 h), after which protein levels stabilize. Similar results were obtained for claudin 7, whereas claudin 2 degrades to ~10% of initial levels (Supplemental Figure S3). In contrast, cyclin D1 degrades completely and rapidly, with a half-life of 35 ± 7min. Exogenously expressed claudin 4 exhibited similar degradation kinetics (Figure 3c). Of interest, IEC barrier properties, as measured by TER, are not perturbed by cycloheximide treatment. Indeed, a significant portion of cellular claudin does not appear to be required for barrier maintenance (Figure 3d and Supplemental Figure S3). To confirm mobile pool depletion, we performed TX-100 detergent extraction of cycloheximide-treated cells (Figure 3e). Under these conditions, TX-100–soluble fractions degrade rapidly, whereas insoluble fractions appear stable. These studies identify a

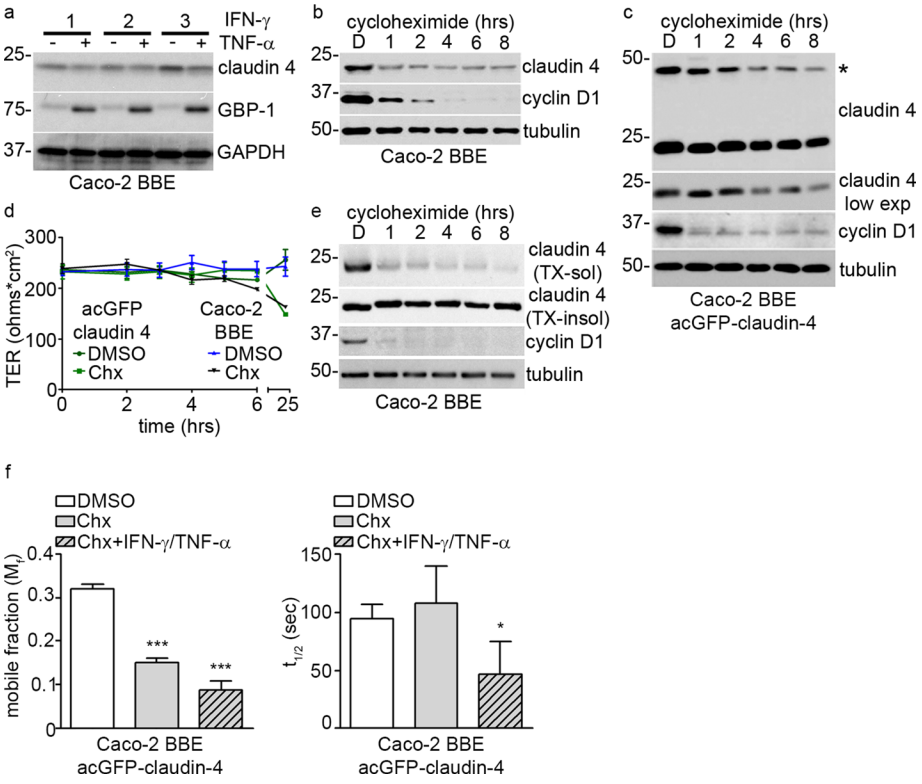

FIGURE 3: IFN-γ/TNF-α exposure decreases the proportion of claudin 4 in the FRAP immobile pool. (a) IFN-γ/TNF-α treatment decreases total claudin 4 protein levels in Caco-2 BBE cells (SEM, $n = 6$, 0.76 ± 0.07 vs. nontreated controls). GBP-1 is included as a positive control for cytokine signaling. (b) Protein synthesis blockage with cycloheximide (Chx, 50 μM) reveals a highly stable endogenous claudin 4 subpool (D, DMSO, 8 h). (c) Exogenous acGFP-claudin 4 (asterisk) protein levels after Chx treatment in Caco-2 BBE cells. (d) TER is not altered by Chx treatment up to 6 h ($n = 3$). (e) TX-100 soluble claudin 4 degrades rapidly after Chx treatment. (f) Caco-2 BBE FRAP analysis of acGFP- claudin 4 recovery 6 h after Chx treatment, with or without 48 h cytokine pretreatment (SEM, $n = 7/10/7$, $^*p < 0.05$, $^{***}p < 0.001$ by ANOVA; all other comparisons are not significant).

highly stable claudin 4 subpool that is sufficient to maintain IEC barrier. However, we did not observe cytokine-induced changes in claudin 4 solubility (Supplemental Figure S3c). We next subjected cycloheximide-treated cells to FRAP analysis. Cycloheximide-treated IECs were dramatically depleted of mobile acGFP-claudin 4 fraction (Figure 3f). Similarly, pretreatment with cytokines contributed to a further decrease in mobile claudin 4. We conclude that the barrier forming, highly-stable claudin 4 subpool represents the FRAP claudin 4 immobile TJ fraction; conversely, mobile claudin 4 has low stability and does not contribute to barrier function. Therefore cytokine treatment reduces the proportion of claudin 4 in the immobile fraction.

Tight junctions are required for cytokine-induced changes in claudin 4 dynamics

The foregoing data show that IFN-γ/TNF-α alter integration of claudin 4 into TJs. Thus our model predicts that cytokine treatment would not affect acGFP-claudin 4 mobility in the absence of organized TJs. To test this hypothesis, we incubated IECs overnight in growth medium containing low calcium (LCM), which resulted in TJ disassembly, disruption of cell–cell contacts, and loss of epithelial barrier function (Figure 4a). Cells cultured in LCM retained acGFP-claudin 4 within the plasma membrane, where it colocalized with F-actin. Cells in LCM were responsive to cytokine treatment, as shown by increased guanylate binding protein 1 (GBP-1) expression (Figure 4b). Monitoring GBP-1 expression served as a positive control for cytokine response (Capaldo *et al.*, 2012). LCM IECs were then subjected to FRAP, both with and without cytokine treatment. As shown in Figure 4C, claudin 4 mobility was unaffected by cytokine exposure in the absence of TJs. Indeed, no significant differences were observed in either the proportion of mobile claudin 4 or the half-life of recovery from bleaching (Figure 4, c and d). acGFP-claudin 4 was transfected into Chinese hamster ovary cells and HeLa cells, which lack TJs even when cultured in normal calcium growth medium. In agreement with the foregoing findings, claudin 4 membrane dynamics in Chinese hamster ovary cells and HeLa cells was similar to that of IECs in LCM (Figure 4, c and d). Taking the results together, we conclude that the mobile claudin 4 subpool has low stability, does not participate in barrier-forming TJs, and has protein dynamics that is not regulated by cytokine signaling. Conversely, FRAP immobile fraction represents claudin 4 that is stably integrated into TJ structures. These observations support a model in which IFN-γ/TNF-α compromises IEC barrier function by decreasing the amount of immobile claudin 4 in the TJ.

Increased claudin 4 protein levels rescue cytokine-induced changes in FRAP dynamics

Cytokine exposure is known to disrupt TJ strand architecture. For example, airway epithelial cells have a decrease in TJ depth and strand number after exposure to proinflammatory cytokines (Coyne *et al.*, 2002). Similar results were found in rat parotid Par-C10 and HT-29/B6 epithelial cells (Schmitz *et al.*, 1999b, Baker *et al.*, 2008). We therefore hypothesized that the observed decrease in claudin 4 immobile fraction would be indicative of changes in TJ strand architecture. The influence of cytokines on organization of TJs was then analyzed by freeze-fracture electron microscopy (Supplemental Figure S5). In contrast to previous studies, gross TJ structure was maintained after cytokine treatment, and the overall strand architecture was similar in control and cytokine-treated IECs. However, an additional TJ strand and occasional strand conformation abnormalities (loops of strands appearing basal to the TJ area) were observed in cytokine-treated IECs (Supplemental Figure S5).

The absence of significant TJ ultrastructural abnormalities was surprising in light of functional barrier compromise in Caco-2 BBE cells after cytokine treatment (Figure 1b). We therefore speculated that both IEC barrier loss and increased claudin 4 protein dynamics resulted from changes in TJ claudin protein composition. Indeed, cytokine exposure correlates with aberrant claudin expression—for example, the decrease in "tight" claudins such as claudin 4 (Figure 3a and Supplemental Figure S4, a and b; Prasad *et al.*, 2005). To investigate the role of claudin 4 protein levels in these processes, we assessed claudin protein dynamics using Caco-2 BBE cells stably

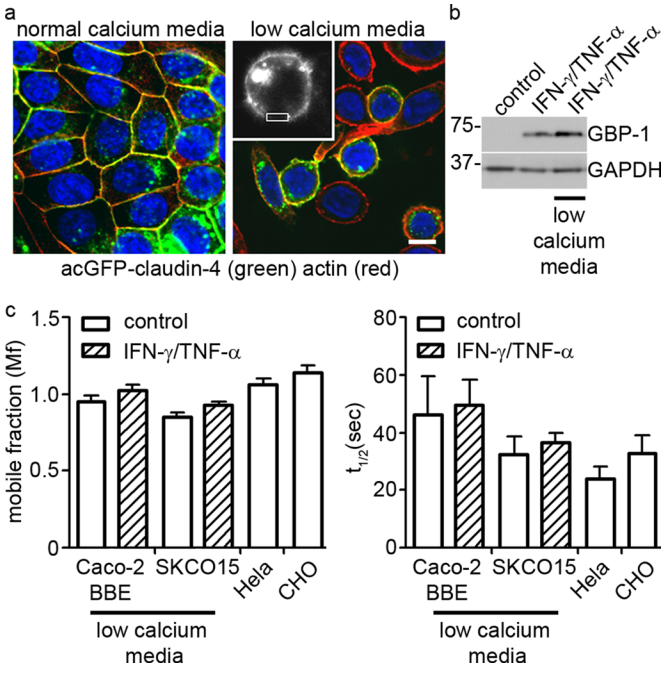

FIGURE 4: TJs are required for cytokine-induced changes in claudin 4 dynamics. (a) Immunofluorescence imaging of SKCO15 acGFP-claudin 4 and actin, demonstrating colocalization under both normal and low-calcium cell culture conditions. Cell–cell contacts are lost in low-calcium conditions, for which cells were subjected to FRAP (ROI, white box, inset; bar, 10 μm). (b) Cytokine signaling is maintained under low-calcium conditions, as demonstrated by high GBP-1 protein levels. (c) SKCO15 FRAP analysis of acGFP-claudin 4 mobility in cells, low-calcium medium. No change in mobility is seen due to IFN-γ/TNF-α stimulation. (d) Mobile fraction and half-time of recovery for Caco-2 BBE and SKCO15 in low-calcium medium, as well as for cells that do not form TJs, HeLa and Chinese hamster ovary cells.

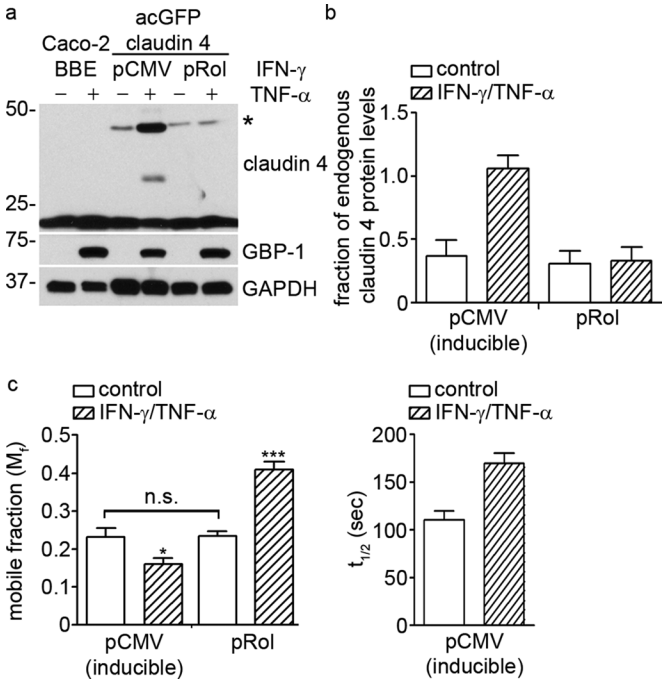

FIGURE 5: Induction of acGFP-claudin 4 expression rescues IFN-γ/TNF-α–induced increases in FRAP dynamics. (a) Western blot analysis of Caco-2 BBE parental cells or cells stably transfected with either pCMV-acGFP-claudin 4 (pCMV) or pRol-acGFP-claudin 4 (pRol). Exogenous acGFP-claudin 4 expression (asterisk) is induced by cytokine treatment in pCMV-acGFP-claudin 4 cells. (b) Densitometric analysis of relative claudin 4 overexpression (exogenous/endogenous). (c) FRAP analysis shows decreased mobile claudin 4 in cells with inducible claudin 4 expression (SEM, $n = 4$; *$p < 0.05$, pCMV IFN-γ/TNF-α vs. control; ***$p < 0.01$, pRol IFN-γ/TNF-α vs. control).

transfected with a cytokine-inducible construct; pCMV-acGFP-claudin 4. The cytomegalovirus (CMV) promoter in this construct contains NFκB-binding sites that are responsive to cytokine exposure, resulting in increased acGFP-claudin 4 expression coincident with IFN-γ/TNF-α treatment (Figure 5a and Supplemental Figure S1). As shown in Figure 5a, cells in which claudin 4 expression is driven from the CMV promoter, when treated with IFN-γ/TNF-α, exhibited elevated levels of exogenous claudin 4 compared with nontreated controls. IFN-γ/TNF-α–induced stimulation of exogenous acGFP-claudin 4 is not observed in IECs transfected with acGFP-claudin 4, where expression is driven by the cytokine-insensitive mutant promoter (Figure 5, a and b, pRol, and Supplemental Figure S1). Analysis of claudin 4 protein mobility by FRAP revealed that increased acGFP-claudin 4 protein levels rescued cytokine-induced change in claudin 4 mobility (Figure 5b). Of interest, the $t_{1/2}$ of claudin 4 recovery was substantially slower than under control conditions (Supplemental Table S1). These findings are in sharp contrast to those in Figure 2, where IFN-γ/TNF-α treatment increased the proportion of mobile claudin 4. We conclude that IFN-γ/TNF-α regulation of acGFP-claudin 4 FRAP dynamics is dependent on claudin 4 protein levels, particularly in directing the proportion of claudin 4 that is integrated into stable TJ.

Claudin 2 and 4 competition contributes to cytokine-induced barrier loss

Because claudin 4 protein levels play a role in TJ dynamics, we next investigated the effects of increased claudin 4 protein levels on cellular claudin protein composition. Cellular claudin composition was assessed under control and cytokine-treated conditions by Western blotting (Figure 6a and Supplemental Figure S4). Previous reports in canine kidney epithelial cells indicate that exogenous expression of claudin 2 is sufficient to decrease both epithelial barrier function and claudin 4 protein levels (Furuse *et al.*, 2001). Furthermore, in HT-29 cells, claudin 4 function has been implicated in rescuing IFN-γ–induced barrier loss (Hering *et al.*, 2011). On the basis of these reports, as well as on our findings, we explored in greater detail the relationship between claudin 2 and 4 protein levels and barrier function. Consistent with previous reports, we identified a reciprocal relationship between the protein levels of claudin 2 and 4, with cytokine-induced increases in claudin 2 and commensurate decreases in claudin 4 (Figure 6a and Supplemental Figure S4). A reciprocal relationship between claudins 2 and 4 was also confirmed by small interfering RNA (siRNA)–mediated depletion of claudin 4, which resulted in increased claudin 2 protein levels (Figure 6b). To assess the effects of claudin 4 protein levels on claudin 2 expression, we sorted stably transfected pCMV-acGFP-claudin 4 Caco-2 BBEs by flow cytometry based on acGFP levels into low, medium, and high acGFP-expressing cell populations (L, M, and H, respectively). Dramatic upregulation of exogenous protein expression was found after cytokine treatment (asterisk in Figure 6, c and d). We then analyzed claudin 2 protein levels in cells that expressed increasing concentration of claudin 4. Indeed, we observed a dose-dependent decrease in claudin 2 protein levels coincident with increasing claudin 4, particularly after cytokine treatment (Figure 6, c and e). Similar findings were observed with claudins 1, 5, and 7 (Supplemental Figure S4). Remarkably, these

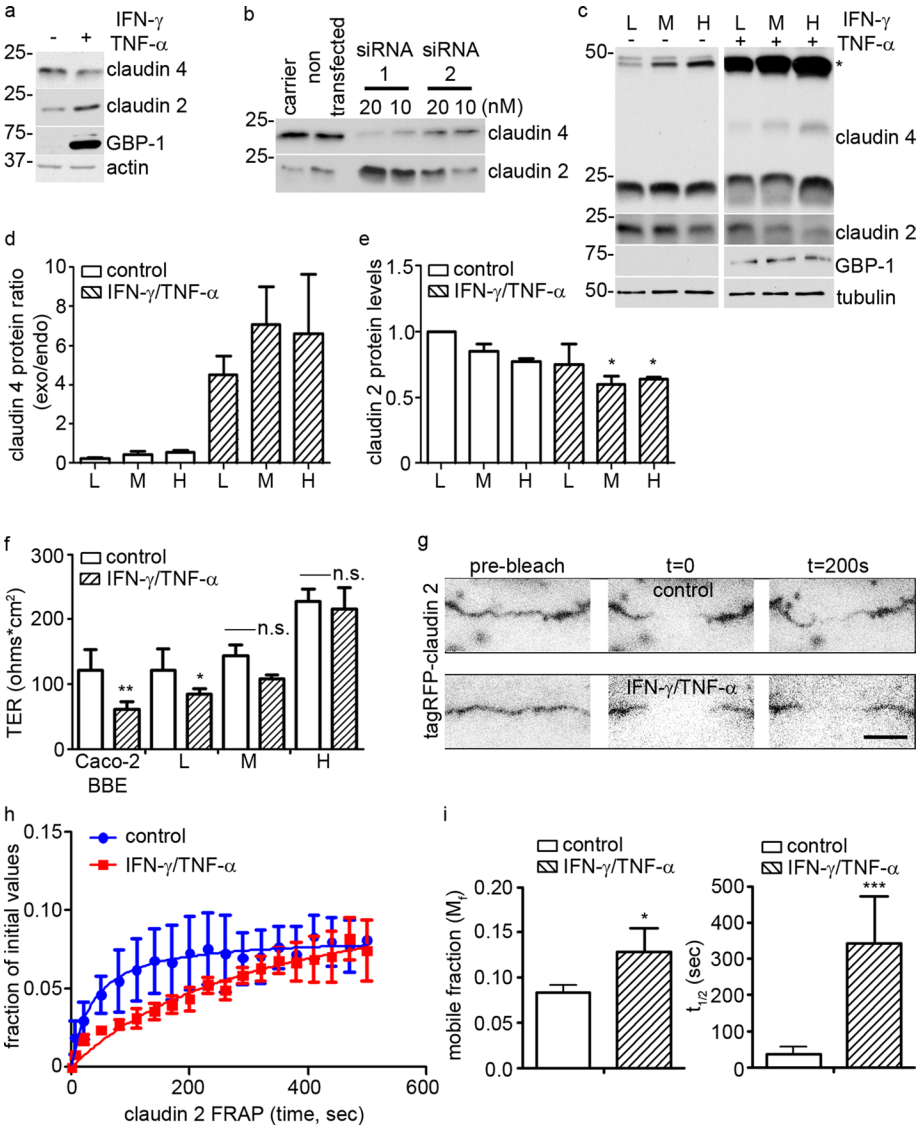

FIGURE 6: Claudin 2/4 exchange exacerbates cytokine-induced barrier loss. (a) parental Caco-2 BBE cells treated with IFN-γ/TNF-α show decreased claudin 4 and increased claudin 2. (b) Reciprocal expression of claudins 2 and 4 after siRNA-mediated suppression of claudin 4. (c) Stable Caco-2 BBE cells (pCMV) sorted for acGFP expression (low, medium, high; L, M, H) and immunoblotted for claudin 4 and 2 (asterisk, exogenous). (d) Densitometric analysis of relative claudin 4 overexpression ($n = 2$, exogenous/endogenous). (e) Densitometric analysis of relative claudin 2 levels ($n = 3$, $^*p < 0.05$ by ANOVA). (f) Claudin 4 overexpression ameliorates IFN-γ/TNF-α–induced loss of IEC barrier function (SEM, $n = 6$, $^{**}p < 0.01$, $^*p < 0.05$ vs. high claudin 4 [$n = 9$] + cytokines; n.s., not significant by ANOVA). (g) tagRFP-Claudin 2 FRAP in nontreated and cytokine-treated conditions. (h) FRAP analysis indicates reduced mobile pool rates for claudin 2 after cytokine treatment. (i) FRAP analysis shows dramatic slowing of claudin 2 recovery in cells after cytokine exposure (SEM, $n = 4/8$, $^*p < 0.05$, $^{***}p < 0.001$, unpaired *t* test).

changes in cellular claudin composition correlated with a progressive resistance to cytokine-induced barrier loss, with high claudin 4–expressing cells showing limited barrier loss (Figure 6f). Given the influence of claudin composition on barrier function, we investigated the dynamics of claudin 2 after cytokine treatment. IECs expressing tagRFP-claudin 2 were subjected to FRAP in either nontreated control conditions or after 48 h of cytokine treatment (Figure 6g). Of interest, claudin 2 contains a lower mobile pool fraction than claudin 4 (0.08 ± .008 vs. 0.27 ± 0.014), and the dynamics of this mobile pool is decreased after cytokine treatment compared with control conditions (Figure 6, h and i). These findings show that cytokine exposure elicits claudin isoform–specific effects on FRAP mobility, with a dramatic slowing of claudin 2 mobility after cytokine treatment.

Heterotypic incompatibility of claudins 2 and 4 determines TJ remodeling after cytokine exposure

Our data indicate that protein levels are a central regulator of both claudin 4 mobility and function. Recent studies have described a potential molecular mechanism that could account for our findings. Claudin isoforms are known to exhibit binding preferences both in-*cis* (within the plasma membrane) and in-*trans* (between opposing cells; Daugherty *et al.*, 2007; Piontek *et al.*, 2011). We therefore evaluated claudin 2/4 incompatibility as a mechanism of cytokine-induced barrier loss. We used HeLa cells as a reductionist model system due to the absence of endogenous claudin expression in these cells. Cell lines were generated that stably expressed either fluorescence-tagged claudin 2 or claudin 4. Confocal microscopy confirmed that the expressed claudins were targeted to the plasma membrane (Figure 7a). Of interest, tagRFP-claudin 2 HeLa cells, when cocultured with acGFP-claudin 4 cells, exhibit a dramatic redistribution of claudin 2 into an intracellular compartment. Consistent with our earlier observations, analysis of heterotypic cell–cell interactions between claudin 2 and 4 cells failed to show claudin accumulation at cell contacts. However, abundant colocalization of claudins 2 and 4 was observed in HeLa cells expressing claudins 2 and 4 in the same cells (Figure 7b). In contrast to our findings in IECs, claudin 2 expressed in HeLa cells exhibited planar diffusion, as shown by kymographic analysis (Figure 7c). This likely indicates that these claudins do not form TJs in HeLa cells. Together these findings show that claudins 2 and 4 are incompatible *trans*-binding partners and interact poorly between adjacent cells.

Heterotypic claudin 2/4 incompatibility presents a mechanism for both cytokine-induced increases in claudin 4 mobility and reduced barrier function; namely, that claudins 2 and 4 compete for TJ integration. Because the foregoing studies were performed in model intestinal epithelial cell lines, we analyzed the relationship of these proteins in primary intestinal epithelial cell cultures. Murine small intestinal epithelial cells were isolated and expanded ex vivo into primary enteroid cultures in a three-dimensional matrix, where they develop as polarized epithelial cysts (Figure 7d). Enteroids under these conditions are similar to intestinal crypt base cells, which express claudin 2 but not claudin 4 protein (Figure 7, d and e). Lentiviral transduction of acGFP-claudin 4 was used to induce its expression in enteroids. As shown in Figure 7,

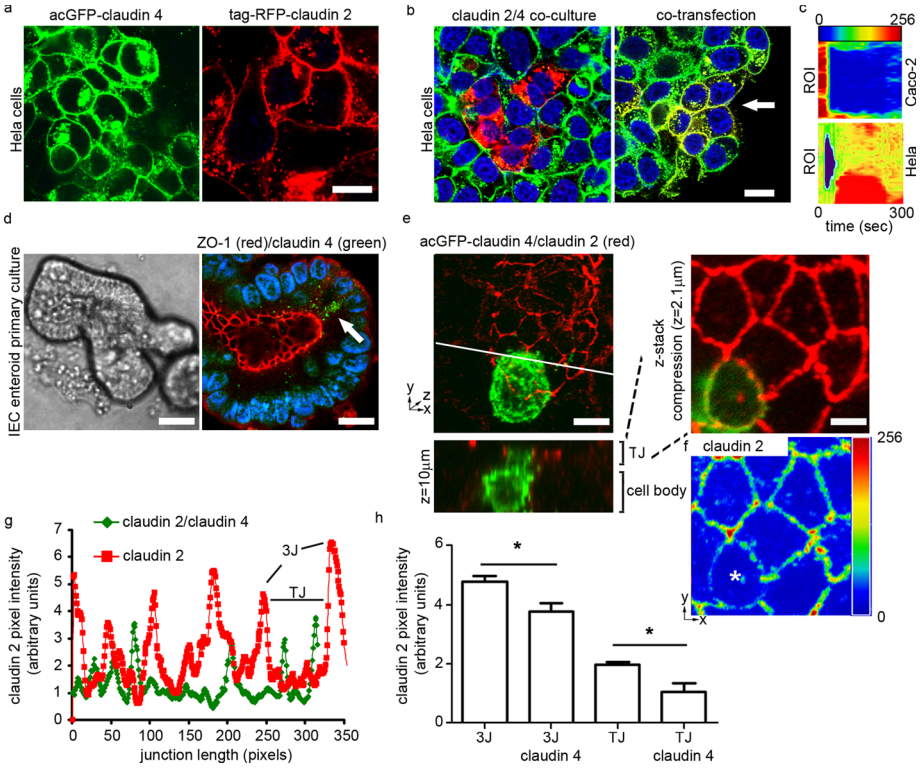

FIGURE 7: Claudin 2/4 transdimer incompatibility regulates claudin membrane localization. (a) HeLa cells do not express endogenous claudins and serve as a reductionistic model of claudin behavior. HeLa cells expressing exogenous acGFP-claudin 4 or tag-RFP-claudin 2. (b) Claudins 2 and 4 do not colocalize in-*trans* (coculture) and yet localize if expressed within the same cell (cotransfection, yellow). (c) Kymograph of HeLa cell ROI FRAP showing rapid planar diffusion of membrane-bound acGFP-claudin 4. This was not seen after Caco-2 ROI FRAP. (d) Enteroid cultures from mouse jejunum do not express claudin 4 at the TJs. Murine enteroids immunostained for ZO-1 (red) and claudin 4 (green). (e) Lentiviral expression of acGFP-claudin 4 displaces claudin 2 from TJ contacts. Left, representative three-dimensional reconstruction of confocal sections. Claudin 2 (red) and acGFP-claudin 4 (green; see Supplemental Video S2). Three *z*-plane sections containing the TJs were compressed for analysis (right). (f) Heat-map of pixel intensities at TJs showing decreased claudin 2 levels in acGFP-claudin 4–expressing cells. (g) Quantitation of claudin 2 levels by pixel intensity analysis by tracing the circumference of the cell at the TJ. (h) Decreased claudin 2 pixel intensities were found at both TJs and tricellular contacts (3J; SEM $n = 12$, $^*p < 0.05$, *t* test).

IECs that expressed claudin 4 in the plasma membrane had reduced claudin 2 in both TJs and tricellular junctions (the intersection of three cells; Figure 7, e–h). Claudin 2 was immunolocalized by confocal microscopy in enteroids transduced to express claudin 4. To evaluate claudin 2 levels at cell contacts, enteroid cysts were processed for immunofluorescence detection and imaged by confocal microscopy. Then *z*-plane confocal sections were used to create three-dimensional reconstructions of epithelial cells in enteroids cysts (Supplemental Video S2). The luminal-facing apical aspect of epithelial cells contain TJ structures, and these *z*-plane sections were excised and compressed, allowing the visualization of TJs en face (Figure 7, e and f). Pixel intensity analysis revealed diminished claudin 2 levels in acGFP-claudin 4–expressing cells (Figure 7, g and h). The foregoing findings support a model in which claudins 2 and 4 compete for position within the TJs of epithelial cells.

DISCUSSION

Proinflammatory cytokine-mediated disruption of mucosal barriers contributes to a multitude of pathological conditions, including inflammatory bowel diseases, bronchial inflammation in asthma and cystic fibrosis, and chronic rhinosinusitis (Coyne *et al.*, 2002; Capaldo and Nusrat, 2009; Den Beste *et al.*, 2013). As a case in point, inflammatory bowel diseases, encompassing Crohn's disease and ulcerative colitis, are characterized by chronic inflammation of the intestinal mucosa, coincident with high levels of the proinflammatory cytokines IFN-γ and TNF-α (Nakamura *et al.*, 1992; Mankertz and Schulzke, 2007). The pathogenesis of inflammatory bowel disease is multifactorial and not well understood. Several lines of evidence implicate a failure to maintain TJ-based paracellular barriers under inflammatory conditions as an important contributing factor to chronic mucosal inflammation and continued epithelial damage (Schmitz *et al.*, 1999a; Laukoetter *et al.*, 2007; Xavier and Podolsky, 2007). Of importance, proinflammatory cytokine exposure of epithelial cells is sufficient to effect changes in TJ claudin composition and barrier function (Capaldo and Nusrat, 2009).

To investigate the molecular mechanisms that underlie TJ remodeling during proinflammatory cytokine exposure, we generated IECs stably expressing acGFP-claudin 4, which serves as a marker of TJ remodeling. We chose to investigate claudin 4 dynamics because it is expressed in TJs of differentiated intestinal epithelial cells, which exhibit tight barrier properties. Furthermore, decreased claudin 4 has been observed in inflamed mucosa (Oshima *et al.*, 2008). Our studies indicate that the proinflammatory cytokines IFN-γ/TNF-α act to regulate TJ integrity by altering the proportional distribution of claudin 4 between mobile and barrier-forming immobile TJ–associated subpools (Figure 8). We contend that this is through competition with claudin 2 for residency within the immobile TJ fraction. Claudin 4 protein levels appear to be key determinants of protein dynamics, barrier function, and cytokine sensitivity. However, it is interesting to note that claudin 4 was previously shown to be heterobinding, incompatible with a number of claudins, including 1, 3, and 5 (Daugherty *et al.*, 2007). This is consistent with our findings in Supplemental Figure S4. Therefore our findings may reflect claudin 4 competition with a number of claudin isoforms. This mechanism should be contrasted with cytokine-induced TJ restructuring, such as internalization of TJ constituents, which occurs after extended cytokine exposure (Bruewer *et al.*, 2003). Taken together, the foregoing findings show that cytokine-induced TJ remodeling results in decreased claudin 4 assembly into TJs that is mediated by incompatibility of claudin isoforms (Figure 8). In the event of increased claudin 2 expression, claudin 4 is excluded from the TJ. Owing to the pore-forming capability of claudin 2, the result is lowered TJ barrier function.

Several studies investigated the dynamics of TJ proteins in live cells by FRAP (Sasaki *et al.*, 2003; Shen *et al.*, 2008; Yamazaki *et al.*, 2011). Our study addressed the relationship between TJ structure/function and TJ protein kinetics. In SF7 cells that lack TJs, expression

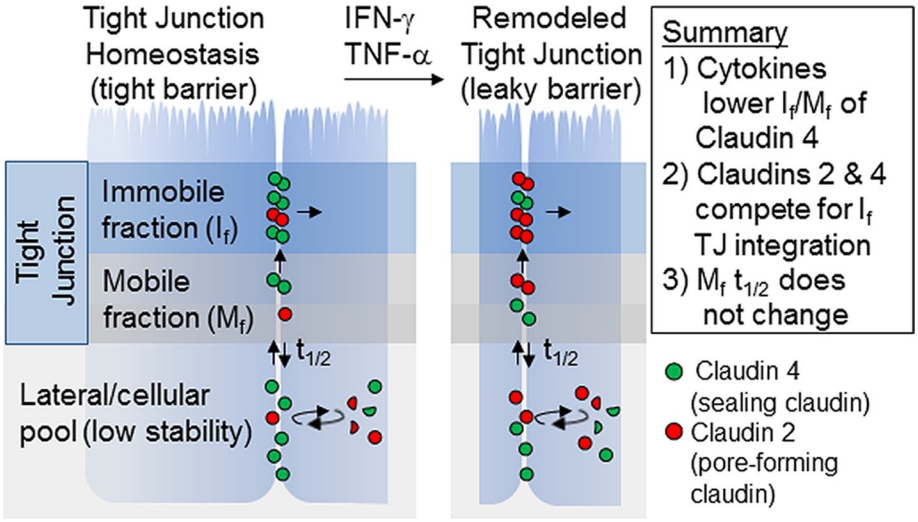

FIGURE 8: Summary of IFN-γ/TNF-α–induced TJ remodeling by claudins 2 and 4. In nontreated control conditions, claudin 4 resides within stable TJ strands with robust barrier properties. IFN-γ/TNF-α treatment displaces a proportion of claudin 4 into a highly mobile/low- stability subpool, where it does not participate in TJ barrier function. This is due to increased expression of incompatible claudin isoforms. Mobile claudin 4 (M_f) exchanges with a lateral/cellular subpool at a rate described by the half-time of recovery ($t_{1/2}$). Immobile subpools (I_f) represent stable, barrier-forming strands. Crescents indicate degraded claudin protein.

of select claudin isoforms produce TJ strands, resulting in unique isoform-specific stand architecture (Yamazaki *et al.*, 2011). These features are complex, and cell type–specific FRAP dynamics were observed for many of the claudin isoforms that have been examined (Yamazaki *et al.*, 2011). Therefore the ultimate determinant of tight junction strand organization and barrier function is likely dependent on the complement of claudins within the cell. To discern mechanisms of IFN-γ/TNF-α–mediated compromise of IEC barrier function, we investigated the nature of FRAP-defined claudin 4 immobile and mobile fractions. Of importance, we did not detect a claudin 4 immobile fraction in TJ-free cell culture systems. These cells fail to form barriers, as determined by TER measurement, and we observed a negative correlation between claudin 4 mobile fraction value and TER. In addition, protein stability assays point to a highly stable subpool of claudin proteins that are sufficient for barrier maintenance. From these data we contend that the FRAP immobile fraction represents TJ-integrated claudin 4, whereas mobile claudin 4 is not TJ associated and does not participate in IEC barrier function. Of importance, exchange between the mobile and immobile subpools was not detected by FRAP at the time scales tested, and further studies will be required to elucidate immobile pool dynamics. However, our study indicates that IFN-γ/TNF-α reduces immobile claudin 4 without influencing its mobile pool dynamics. This is in contrast to the TJ protein occludin, whose mobility in the presence of TNF-α increases without a significant change in the mobile/immobile fraction distribution (Buschmann *et al.*, 2013). Unlike claudin 4, analysis of the pore-forming claudin 2 FRAP mobility revealed that cytokine treatment decreases claudin 2 mobile pool dynamics. These findings suggest that cytokines have differential effects on mobility of claudin proteins in TJs.

Current theories concerning the molecular mechanisms of cytokine-mediated TJ compromise include disruption of Rho/MLC-dependent actin contractility and claudin exchange (Capaldo and Nusrat, 2009). Recent studies of TJ protein FRAP dynamics suggest a close interplay between actin tension and TJ mobility (Yu *et al.*, 2010). Actin tension also plays a significant role in cytokine-induced TJ restructuring (Wang *et al.*, 2005; Capaldo and Nusrat, 2009; Ivanov *et al.*, 2009). Although we have not tested a role for actin contractility in the regulation of claudin 4 mobility, our data suggest a prominent role for claudin exchange in inflammation-induced TJ dysfunction. Of interest, depletion of claudin 4 by siRNA results in a striking increase in claudin 2. Complementary findings indicate that exogenous expression of claudin 4 decreases claudin 2 levels. Conversely, IFN-γ/TNF-α treatment results in an increase in claudin 2 and a decrease in claudin 4. These findings lead us to conclude that, in Caco-2 BBE cells, balanced claudin 2/4 protein expression is required to maintain TJ barrier homeostasis. Previous studies described protein–protein interaction preferences by claudin isoforms. Indeed, our studies show that, in HeLa cells, claudin 2 does not accumulate with claudin 4 at TJs. We contend that this is due to incompatible extracellular heterotypic interactions. Claudin 4 has only been shown to exhibit homotypic interactions. In addition, incompatibility in *trans*-binding regulates subpool partitioning and subsequent TJ strand incorporation. In theory, by increasing protein levels of claudin 4 in cytokine-treated cells, we are enhancing the probability of forming claudin 4 homotypic interactions. Finally, HeLa cell FRAP studies show planar diffusion of acGFP-claudin 4 and similar mobile pool dynamics to that observed in TJ-free systems such as calcium-switch FRAP assays. These may indicate that claudin 2/4 incompatibility occurs at some point before TJ assembly.

Taken together, our findings show that TJ remodeling by proinflammatory cytokines acts through decreased long-term kinetics of claudin 4 assembly into TJs, thereby impairing IEC barrier function. In conclusion, TJ remodeling occurs after cytokine exposure through mechanisms of heterotypic 2/4 claudin incompatibility. Claudin sorting at the TJ by heterobinding preferences is consistent with the concept of TJs as self-assembling systems.

MATERIALS AND METHODS

FRAP microscopy

FRAP was performed on fluorescent claudin–expressing cells (with or without IFN-γ/TNF-α treatment, 100 U/ml/10 ng/ml, 48 h) using a Nikon A1R confocal microscope with temperature control/CO_2 chamber stage (60× oil lens, numerical aperture 1.4). ROI pixel intensities were recorded with NIS-Elements AR 4.0 software (Nikon, Melville, NY). FRAP conditions used in the analysis include 1) FRAP of TJ between adjacent claudin-expressing cells, 2) 4-s bleach, 3) 80 ± 10% photobleach of initial intensity, 4) maintenance of *z*-plane resolution throughout assay, 5) correction for bleaching due to imaging conditions, and 6) adjustment of recovery maxima to estimate the fraction of total fluorophore bleached. Data were analyzed using ImageJ (National Institutes of Health, Bethesda, MD).

In silico TJ modeling

Mathematical modeling of FRAP pixel intensity was performed using Prism (GraphPad, La Jolla, Ca). FRAP was modeled as follows: pixel intensity $I_t = (I_0 + (I_{max}t/t_{1/2}))/(1 + t/t_{1/2})$ (Shen *et al.*, 2008). The mobile and immobile fractions were calculated as $M_f = (I_{max} - I_0)/(1 - I_0)$ and

I_f (fraction that is stable in the TJ) = 1 − M_f, respectively. The FRAP model was applied after time t_0, and postbleach intensities (I_0) were set as baseline. Best-fit curves were generated for experimental and control samples and evaluated by goodness-of-fit analysis. Half-life of recovery ($t_{1/2}$) and I_{max} values were then determined by nonlinear regression analysis.

Stable cell lines

Cells were transfected with Lipofectamine 2000 reagent (Invitrogen, Carlsbad, CA). IECs with pCMV-acGFP-claudin 4 cells were a gift from David Lo, University of California, Riverside. Claudin-expressing vectors were linearized, transfected into various cell lines (SKCO15, Caco-2 BBE, HeLa, Chinese hamster ovary), and cultured in selection media. GFP-expressing cells are sorted at the Emory University Cell-Sorting Facility.

Primary murine IEC enteroid cultures

Mouse intestine (jejunum) was dissected and flushed with phosphate-buffered saline (PBS) and transferred to chelation buffer (2 mM EDTA, PBS) for 30 min. The intestine was shaken to remove crypt cells and then incubated in PBS with 43 mM sucrose and 55 mM sorbitol and filtered through a 70-μm filter. Crypts were resuspended in Matrigel (BD Bioscience, San Jose, CA) containing 50 ng/ml epidermal growth factor (R&D Systems, Minneapolis, MN), 100 ng/ml Noggin (R&D Systems), and 500 ng/ml R-spondin (R&D Systems). Crypts were then incubated in DMEM/F12 with N2 and B27 supplement (R&D Systems, Invitrogen, Life Technologies, Grand Island, NY). All experimental protocols used male C57BL/6 mice (Jackson Laboratory, Bar Harbor, ME). All procedures using animals were reviewed and approved by the Emory University Institutional Animal Care and Use Committee and were performed according to National Institutes of Health criteria.

Freeze-fracture electron microscopy

In a blinded study, freeze-fracture electron microscopy was performed on cells grown on permeable supports that were fixed with phosphate-buffered glutaraldehyde (2%). Preparations were incubated in 10% (vol/vol) and then in 30% (vol/vol) glycerol and finally frozen in liquid nitrogen–cooled Freon 22. Cells were fractured at −100°C and shadowed with platinum and carbon in a vacuum evaporator (Denton DV-502, Moorestown, NJ). Replicas were bleached with sodium hypochloride, picked up on grids, and analyzed with a video-equipped Zeiss 902A electron microscope (Carl Zeiss AG, Thornwood, NY; Olympus iTEM Veleta, Shinjuku, Tokyo, Japan). Morphometric analysis was performed at a final magnification of 51,000×. Vertical grid lines were drawn at 200-nm intervals perpendicular to the most apical TJ strand. The strands horizontally oriented within the main TJ meshwork were counted at intersections with grid lines. The distance between the most apical and the contra-apical strand was measured as the meshwork depth. Strand discontinuities within the main compact TJ meshwork of >20 nm were defined as "breaks" and given per micrometer length of horizontally oriented strands. Strand formation was noted as "particle type" or "continuous type." The pattern of strand loops was denoted as "angular type" or "curved type." Because non-Gaussian distribution occurred, the results were tested for significance using the Wilcoxon–Mann–Whitney test.

Antibodies and reagents

Cytokines IFN-γ and TNF-α were from Genentech (San Francisco, CA) and Peprotech (Rocky Hill, NJ), respectively. Claudin 2/4/7 and cyclin D1 half-life was determined after cycloheximide treatment (50 μM, 0–8 h). siRNA for claudin 2, 00034695, and claudin 4, 00189579 (Sigma-Aldrich, St. Louis, MO). Western blot and immunofluorescence (IF) analysis antibodies include protein loading controls (glyceraldehyde-3-phosphate dehydrogenase [Sigma-Aldrich], actin [Sigma-Aldrich], and α-tubulin [Invitrogen]), TJ molecules (claudins 1, 2, 4, 5, and 7 [Invitrogen], occludin [Invitrogen], Jam-A [created in this lab], and ZO-1/2 [Invitrogen]), adherens junction molecules (E-cadherin [Sigma-Aldrich] and β-catenin [Sigma-Aldrich]), GBP-1 as a control for cytokine stimulation (Santa Cruz Biotechnology, Santa Cruz, CA), and horseradish peroxidase (HRP)/fluorophore-linked secondary antibodies (Invitrogen, Jackson ImmunoResearch, West Grove, PA).

Immunofluorescence staining and microscopy

Cells were fixed in 3.7% paraformaldehyde or 100% methanol for 20 min. Primary antibody reactions were performed in Hank's balanced salt solution$^{+/+}$ with 3% bovine serum albumin (BSA) for 1 h. Secondary antibodies (Alexa Fluor 546 conjugated) were incubated in 3% BSA and for 45 min. Nuclei were detected with TOPRO-3. Confocal microscopy was performed using a Zeiss LSM 510 microscope (Carl Zeiss).

Western blot analysis

Cells were lysed in lysis buffer (50 mM Tris, pH 6.8, 10% glycerol, 2% SDS) supplemented with phosphatase inhibitor cocktails I and II and protease inhibitor cocktail (Sigma-Aldrich), incubated at 60°C for 30 min, and subjected to SDS–PAGE. Primary antibodies were incubated for 1 h at room temperature, followed by a 3× wash with TTBS (0.1% Tween 20, 50 mM Tris-Cl, and 150 mM NaCl). HRP-conjugated secondary antibodies were incubated at room temperature for 45 min. TX-100 extraction was performed as previously described (Bruewer *et al.*, 2003). Insoluble fractions were then processed as described earlier.

Transepithelial electrical resistance

IECs were grown on permeable supports, and monolayers were monitored for electrical resistance using an epithelial volt-ohmmeter (EVOM/EndOhm; World Precision Instruments, Sarasota, FL).

Constructs

Lentivirus was produced in HEK293TLA cells by transfection of pLex-acGFP-claudin 4 or pLex-acGFP with viral packaging vector pSPAX2 and pMD2.G. Virus was harvested after 48 h and concentrated by ultracentrifugation at 83,000 × *g* for 2 h and titered as described (Salmon and Trono, 2006). Site-directed mutagenesis was conducted on pcDNA3.1 hygro as described previously (Gustems *et al.*, 2006).

Statistics

Statistics was performed as indicated. One-way analysis of variance (ANOVA) included Bonferroni posttest, Student's *t* test, or Wilcoxon–Mann–Whitney test as indicated. Error is reported as SEM.

ACKNOWLEDGMENTS

We thank David Lo for providing the pCMV-acGFP claudin 4 Caco-2 BBE cells, Noah Shroyer for assistance with enteroid cultures, and Oskar Laur at the Emory Cloning Core, Robert Karaffa at the Emory University Flow Cytometry Core Facility, and Mike Kwon, In-Fah Lee, and Jeff Vallance for expert technical assistance. Supported by the National Institutes of Health (DK64399 to C.A.P.; DK55679 and

DK59888 to A.N.; HL116958 to M.K.; and DK64399 [National Institutes of Health DDRC grant]), Emory University Integrated Cellular Imaging Microscopy Core of the Winship Cancer Institute Comprehensive Cancer Center Grant P30CA138292, a Crohn's and Colitis Foundation of America Career Development award to C.T.C. and a fellowship award to A.E.F., and Deutsche Forschungsgemeinschaft FOR 721 TP-Z to S.M.K. and M.F.

REFERENCES

Anderson JM, Van Itallie CM (2009). Physiology and function of the tight junction. Cold Spring Harbor Perspect Biol 1, a002584.

Baker OJ, Camden JM, Redman RS, Jones JE, Seye CI, Erb L, Weisman GA (2008). Proinflammatory cytokines tumor necrosis factor-alpha and interferon-gamma alter tight junction structure and function in the rat parotid gland Par-C10 cell line. Am J Physiol Cell Physiol 295, C1191–C1201.

Bruewer M, Luegering A, Kucharzik T, Parkos CA, Madara JL, Hopkins AM, Nusrat A (2003). Proinflammatory cytokines disrupt epithelial barrier function by apoptosis-independent mechanisms. J Immunol 171, 6164–6172.

Buschmann MM, Shen L, Rajapakse H, Raleigh DR, Wang Y, Wang Y, Lingaraju A, Zha J, Abbott E, McAuley EM, *et al*. (2013). Occludin OCEL-domain interactions are required for maintenance and regulation of the tight junction barrier to macromolecular flux. Mol Biol Cell 24, 3056–3068.

Capaldo CT, Beeman N, Hilgarth RS, Nava P, Louis NA, Naschberger E, Sturzl M, Parkos CA, Nusrat A (2012). IFN-gamma and TNF-alpha-induced GBP-1 inhibits epithelial cell proliferation through suppression of beta-catenin/TCF signaling. Mucosal Immunol 5, 681–690.

Capaldo CT, Nusrat A (2009). Cytokine regulation of tight junctions. Biochim Biophys Acta 1788, 864–871.

Chavez AM, Morin MJ, Unno N, Fink MP, Hodin RA (1999). Acquired interferon gamma responsiveness during Caco-2 cell differentiation: effects on iNOS gene expression. Gut 44, 659–665.

Claude P, Goodenough DA (1973). Fracture faces of zonulae occludentes from "tight" and "leaky" epithelia. J Cell Biol 58, 390–400.

Coyne CB, Vanhook MK, Gambling TM, Carson JL, Boucher RC, Johnson LG (2002). Regulation of airway tight junctions by proinflammatory cytokines. Mol Biol Cell 13, 3218–3234.

Daugherty BL, Ward C, Smith T, Ritzenthaler JD, Koval M (2007). Regulation of heterotypic claudin compatibility. J Biol Chem 282, 30005–30013.

Den Beste KA, Hoddeson EK, Parkos CA, Nusrat A, Wise SK (2013). Epithelial permeability alterations in an in vitro air-liquid interface model of allergic fungal rhinosinusitis. Int Forum Allergy Rhinol 3, 19–25.

Furuse M (2010). Molecular basis of the core structure of tight junctions. Cold Spring Harb Perspect Biol 2, a002907.

Furuse M, Furuse K, Sasaki H, Tsukita S (2001). Conversion of zonulae occludentes from tight to leaky strand type by introducing claudin-2 into Madin-Darby canine kidney I cells. J Cell Biol 153, 263–272.

Gilham DE, Lie ALM, Taylor N, Hawkins RE (2010). Cytokine stimulation and the choice of promoter are critical factors for the efficient transduction of mouse T cells with HIV-1 vectors. J Gene Med 12, 129–136.

Gustems M, Borst E, Benedict CA, Perez C, Messerle M, Ghazal P, Angulo A (2006). Regulation of the transcription and replication cycle of human cytomegalovirus is insensitive to genetic elimination of the cognate NF-kappaB binding sites in the enhancer. J Virol 80, 9899–9904.

Hering NA, Andres S, Fromm A, van Tol EA, Amasheh M, Mankertz J, Fromm M, Schulzke JD (2011). Transforming growth factor-beta, a whey protein component, strengthens the intestinal barrier by upregulating claudin-4 in HT-29/B6 cells. J Nutr 141, 783–789.

Hering NA, Fromm M, Schulzke JD (2012). Determinants of colonic barrier function in inflammatory bowel disease and potential therapeutics. J Physiol 590, 1035–1044.

Ivanov AI, Samarin SN, Bachar M, Parkos CA, Nusrat A (2009). Protein kinase C activation disrupts epithelial apical junctions via ROCK-II dependent stimulation of actomyosin contractility. BMC Cell Biol 10, 36.

Kline JN, Hunninghake GM, He B, Monick MM, Hunninghake GW (1998). Synergistic activation of the human cytomegalovirus major immediate early promoter by prostaglandin E2 and cytokines. Exp Lung Res 24, 3–14.

Laukoetter MG, Nava P, Lee WY, Severson EA, Capaldo CT, Babbin BA, Williams IR, Koval M, Peatman E, Campbell JA, *et al*. (2007). JAM-A regulates permeability and inflammation in the intestine in vivo. J Exp Med 204, 3067–3076.

Mankertz J, Schulzke JD (2007). Altered permeability in inflammatory bowel disease: pathophysiology and clinical implications. Curr Opin Gastroenterol 23, 379–383.

Mitchell LA, Overgaard CE, Ward C, Margulies SS, Koval M (2011). Differential effects of claudin-3 and claudin-4 on alveolar epithelial barrier function. Am J Physiol Lung Cell Mol Physiol 301, L40–49.

Nakamura M, Saito H, Kasanuki J, Tamura Y, Yoshida S (1992). Cytokine production in patients with inflammatory bowel disease. Gut 33, 933–937.

Oshima T, Miwa H, Joh T (2008). Changes in the expression of claudins in active ulcerative colitis. J Gastroenterol Hepatol 23(Suppl 2), S146–S150.

Piontek J, Fritzsche S, Cording J, Richter S, Hartwig J, Walter M, Yu D, Turner JR, Gehring C, Rahn HP, *et al*. (2011). Elucidating the principles of the molecular organization of heteropolymeric tight junction strands. Cell Mol Life Sci 68, 3903–3918.

Piontek J, Winkler L, Wolburg H, Muller SL, Zuleger N, Piehl C, Wiesner B, Krause G, Blasig IE (2008). Formation of tight junction: determinants of homophilic interaction between classic claudins. FASEB J 22, 146–158.

Prasad S, Mingrino R, Kaukinen K, Hayes KL, Powell RM, Mac Donald TT, Collins JE (2005). Inflammatory processes have differential effects on claudins 2, 3 and 4 in colonic epithelial cells. Lab Invest 85, 1139–1162.

Rahner C, Mitic LL, Anderson JM (2001). Heterogeneity in expression and subcellular localization of claudins 2, 3, 4, and 5 in the rat liver, pancreas, and gut. Gastroenterology 120, 411–422.

Raleigh DR, Boe DM, Yu D, Weber CR, Marchiando AM, Bradford EM, Wang Y, Wu L, Schneeberger EE, Shen L, *et al*. (2011). Occludin S408 phosphorylation regulates tight junction protein interactions and barrier function. J Cell Biol 193, 565–582.

Salmon P, Trono D (2006). Production and titration of lentiviral vectors. Curr Protoc Neurosci Chapter 4, Unit 4.21.

Sasaki H, Matsui C, Furuse K, Mimori-Kiyosue Y, Furuse M, Tsukita S (2003). Dynamic behavior of paired claudin strands within apposing plasma membranes. Proc Natl Acad Sci USA 100, 3971–3976.

Schmitz H, Barmeyer C, Fromm M, Runkel N, Foss HD, Bentzel CJ, Riecken EO, Schulzke JD (1999a). Altered tight junction structure contributes to the impaired epithelial barrier function in ulcerative colitis. Gastroenterology 116, 301–309.

Schmitz H, Fromm M, Bentzel CJ, Scholz P, Detjen K, Mankertz J, Bode H, Epple HJ, Riecken EO, Schulzke JD (1999b). Tumor necrosis factor-alpha (TNFalpha) regulates the epithelial barrier in the human intestinal cell line HT-29/B6. J Cell Sci 112, 137–146.

Shen L, Weber CR, Raleigh DR, Yu D, Turner JR (2011). Tight junction pore and leak pathways: a dynamic duo. Annu Rev Physiol 73, 283–309.

Shen L, Weber CR, Turner JR (2008). The tight junction protein complex undergoes rapid and continuous molecular remodeling at steady state. J Cell Biol 181, 683–695.

Tsukita S, Furuse M (2002). Claudin-based barrier in simple and stratified cellular sheets. Curr Opin Cell Biol 14, 531–536.

Van Itallie C, Rahner C, Anderson JM (2001). Regulated expression of claudin-4 decreases paracellular conductance through a selective decrease in sodium permeability. J Clin Invest 107, 1319–1327.

Wang F, Graham WV, Wang Y, Witkowski ED, Schwarz BT, Turner JR (2005). Interferon-gamma and tumor necrosis factor-alpha synergize to induce intestinal epithelial barrier dysfunction by up-regulating myosin light chain kinase expression. J Pathol 166, 409–419.

Wray C, Mao Y, Pan J, Chandrasena A, Piasta F, Frank JA (2009). Claudin-4 augments alveolar epithelial barrier function and is induced in acute lung injury. J Physiol Lung Cell Mol Physiol 297, L219–227.

Xavier RJ, Podolsky DK (2007). Unravelling the pathogenesis of inflammatory bowel disease. Nature 448, 427–434.

Yamazaki Y, Tokumasu R, Kimura H, Tsukita S (2011). Role of claudin species-specific dynamics in reconstitution and remodeling of the zonula occludens. Mol Biol Cell 22, 1495–1504.

Yu D, Marchiando AM, Weber CR, Raleigh DR, Wang Y, Shen L, Turner JR (2010). MLCK-dependent exchange and actin binding region-dependent anchoring of ZO-1 regulate tight junction barrier function. Proc Natl Acad Sci USA 107, 8237–8241.

Zeissig S, Burgel N, Gunzel D, Richter J, Mankertz J, Wahnschaffe U, Kroesen AJ, Zeitz M, Fromm M, Schulzke JD (2007). Changes in expression and distribution of claudin 2, 5 and 8 lead to discontinuous tight junctions and barrier dysfunction in active Crohn's disease. Gut 56, 61–72.